The following conclusions can be drawn from the above study: (1) Pyrolysis of phosphoric acid pretreated viscose rayon cloth under a carbon dioxide atomosphere leads to widening of pores above MHTT 850°C. (2) In the case of chars prepared under a nitrogen atmosphere, pre-treatement of the precursor with phosphoric acid tends to inhibit sintering of the pores even at high temperatures.

Acknowledgments - The authors are thankful to Dr. Krishan Lal, Head, Material Characterization Division and Prof. E.S.R. Gopal, Director, National Physical Laboratory, New Delhi,India, for their kind permission to publish this paper. The authors are also thankful to Mr. R.K. Saxena for his keen interest in the experimental work.

REFERENCES

1. Suzuki, M., *Carbon,* 1994, **32**, 577.
2. Bailey, A. and Maggs, F.A.P., Br. Patent No. 1310101, 1971.
3. Bailey, A., Maggs, F.A.P. and Wiliams, J.H., Br. Patent No. 1310011, 1973.
4. Maggs, F.A.P., Smith, M.E. and Robins, G.A., *Proc. 13th Biennial Conf. Carbon,* 1977, Irvine, CA., pp 3-4.
5. Djuricic, Lj., Polovina, M. and Marinkovic, S., *Proc. Carbon'80,* Baden-Baden, pp. 193-6,
6. Capon, A., Alves, B.R. , Smith, M.E and White, M.P., *Proc. 15th Biennial Conf. Carbon,* 1981, Philadelphia, PA, pp. 259-9.
7. Badami, D.V., Compbell, C., Davy, A.D., and Lindsey, M.J., *Proc. Second Conf. Indust. Carbon and Graphite,* 1966, Soc. Chem. Ind., p.48.
8. Carrot, P.J.M. and Freeman, J.J., *Carbon,* 1991, **29**, 499.
9. Bohra, J.N. , Awasthy, B.R. and Chari, S.S., *Fibre Sci. and Technol.,* 1981, **14**, 221.
10. Brunner, P. H. and Roberts, P. V. *Carbon,* 1980, **18**, 217.
11. Indian Standard: Method for determination of specific surface area of powders and porous particles, using low temperature gas adsorption techniques, IS:11578. 1986.
12. Gregg, S.J. and Sing, K.S.W., *Adsorption, Surface Area and Porosity,* Academic Press Inc. London, 1982, p. 214.
13. Rodriguez-Reinoso, F., Linares-Solano, A., Martin-Martinez, J.M. and Lopez-Gonzalez, J.D., *Carbon,* 1984, **22**, 123.
14. Garrido, J., Linares-Solano, A., Martin-Martinez, J.M., Molina-Sabio, M., Rodriguez-Reinoso, F. and Torregrosa, R., *J. Chem. Soc., Faraday Trans.* 1987, **I 83**, 1081.
15. Martin-Martinez, J.M. Molina-Sabio, M., Rodriguez -Reinoso, F. and Torregrosa, R., *Fuel,* 1989, **68**, 204.
16. Mittelmeijer-Hazeleger, M.C. and Martin-Martinez, J.M., *Carbon,* 1992, **30**, 695.
17. Molina-Sabio, M., Rodriguez-Reinoso, F., Caturla, F., and Selles, M.J., *Carbon,* 1995, **33**, 1105.

Electromechanical behavior of carbon fiber

XIAOJUN WANG and D.D.L. CHUNG
Composite Materials Research Laboratory, State University of New York at Buffalo
Buffalo, NY 14260-4400

(Received 1 July 1996; accepted in revised form 24 February 1997)

Key Words - A. carbon fiber, D. electrical properties, elastic properties, mechanical properties

Due to the importance of carbon fibers for structural composites, much attention has been given to the mechanical properties of carbon fibers. Considerable attention has also been given to the electrical properties of carbon fibers, because the electrical properties shed light on the electronic structure and are relevant to the electromagnetic interference shielding effectiveness and lightning protection of carbon fiber composites. However, little attention has been given to the electromechanical behavior, which refers to the electrical behavior as affected by mechanical stress [1-5]. The electromechanical behavior is relevant to the use of a carbon fiber as a strain/stress sensor and to the ability of a carbon fiber composite to sense its own strain/stress and damage [6]. Due to the importance of sensing in smart structures and the close relationship between strain/stress sensing and the electromechanical behavior, the electromechanical behavior of materials is of much current interest. Furthermore, study of the electromechanical behavior provides fundamental information on the effect of stress on the structure of the material. For these reasons, this paper addresses the electromechanical behavior of carbon fibers.

Previous electromechanical study of carbon fibers reported that, for low-modulus carbon fibers, the electrical resistance increases reversibly with tensile strain and decreases reversibly with compressive strain, mainly due to dimensional change rather than resistivity change [1-5]. However, fiber damage must occur at high strains prior to fracture and damage is expected to cause the fiber resistivity to increase irreversibly, though the irreversible effect was not investigated in previous work. The practical implication is that an irreversible resistivity increase in the fiber may be used as an indicator of fiber damage. The objective of this paper is to investigate the correlation between irreversible resistivity increase, irreversible strain and elastic modulus decrease, so as to evaluate the effect of fiber damage on the fiber resistivity.

The carbon fiber used was 10E-Torayca T-300 (unsized, PAN-based), diam. 7 mm, density 1.76 g/cm^3, tensile modulus 221 ± 4 GPa, tensile strength 3.1 ± 0.2 GPa and ultimate elongation 1.4%. The electrical resistivity was (2.2 ± 0.5) x 10^{-3} Ω.cm, as measured by using the four-probe method and silver paint electrical contacts on single fibers. Single fiber electromechanical testing was conducted by measuring the electrical resistance during static and cyclic tension. The DC resistance was measured by using the four-probe method, using silver paint for the electrical contacts. The outer two contacts (50 mm apart) were for passing a current; the inner two contacts (40 mm apart) were for

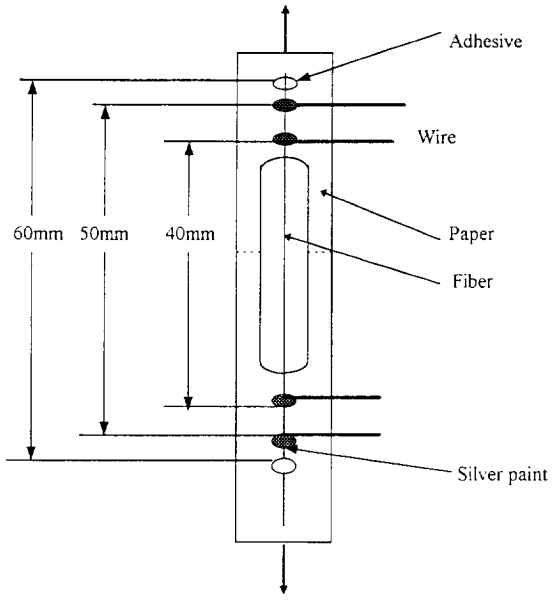

Fig. 1 Configuration for single fiber electromechanical testing. The single fiber (solid vertical line) is adhered to a sheet of paper (shaded area) using adhesive (dotted circles) such that the points of adhesion are 40 mm apart. The four silver paint electrical contacts (small rectangles) are such that the outer contacts are 34 mm apart and the inner contacts are 14 mm apart. The sheet of paper has a rectangular hole cut in its middle. The inner contacts are within the hole.

voltage measurement (Fig. 1). A Keithley 2001 multimeter was used. Away from the four contacts, the single fiber was attached vertically with adhesive (60 mm apart) to a piece of paper with a rectangular hole cut in it. Prior to vertical tension application, the paper was cut horizontally along the dashed lines shown in the figure. The tension was under load control, as provided by a screw-type mechanical testing system (Sintech 2/D). The crosshead speed was 0.1 mm/min. The strain was obtained from the crosshead displacement.

Fig. 2 shows typical plots of the fractional increase in resistance ($\Delta R/R_o$), stress and strain simultaneously obtained during static tensile testing to

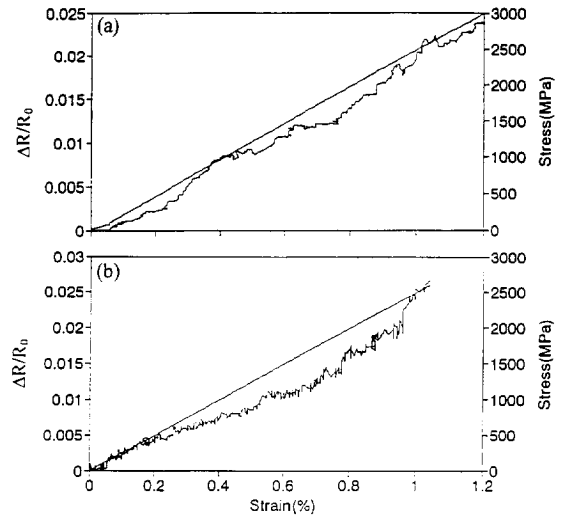

Fig. 2 DR/R_o, stress and strain simultaneously obtained during static tension up to failure.

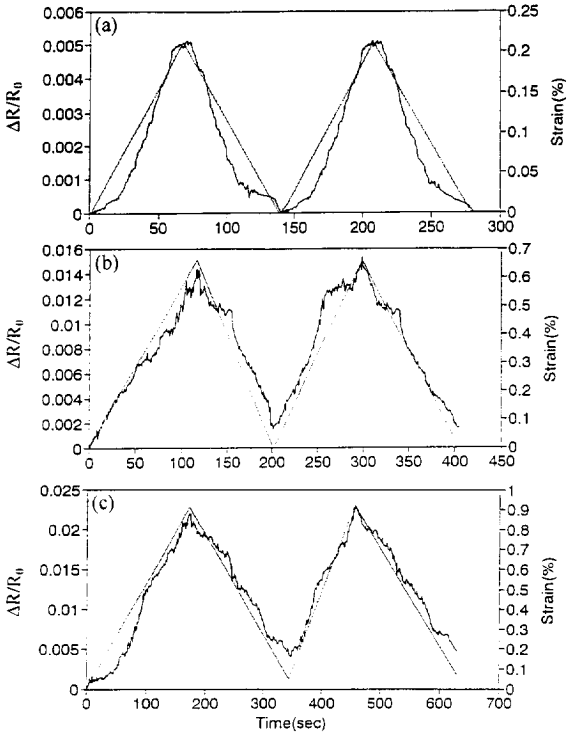

Fig. 3 Plots of DR/R_o vs. time and of strain vs. time during two cycles of cyclic tension at a maximum stress of (a) 18.8% of the fracture stress, (b) 58.1% of the fracture stress and (c) 83.0% of the fracture stress.

failure. $\Delta R/R_o$ increased monotonically with strain/ stress, with a slight negative deviation from linearity. The extent of negative deviation varied from sample to sample. About 10% of the samples were anomalous in that $\Delta R/R_o$ decreased a little before increasing monotonically. This anomaly was also reported in [1]. Table 1 shows the analysis of the results in Fig. 2a. The strain sensitivity, given by the measured $\Delta R/R_o$ divided by the strain, was 1.8 - 1.9 throughout the whole strain range. The $\Delta R/R_o$ calculated from the change in dimensions was less than, but quite close to, the measured $\Delta R/R_o$ at every strain value.

Fig. 3 shows plots of $\Delta R/R_o$ vs. time and strain vs. time, simultaneously obtained during the first 2 cycles of tensile loading at stress amplitudes equal to 18.8%, 58.1% and 83.0% of the fracture stress respectively. Table 2 shows the analysis of such results for five values of the stress amplitude. The strain and $\Delta R/R_o$ were totally reversible at low values of the stress amplitude (up to 58.1% of the fracture stress), but their irreversible components increased with stress amplitude at high values of the stress amplitude. At the highest stress amplitude of 83.0% of the fracture stress, the extent of irreversibility of strain and $\Delta R/R_o$ increased slightly with cycle number (Fig. 3c and Table 2). At the intermediate stress amplitude of 58.1% of the fracture stress, the strain was totally reversible but $\Delta R/R_o$ was not (Fig. 3b). A nonzero irreversible portion of $\Delta R/R_o$ was associated with a nonzero fractional decrease in the elastic modulus from the first cycle to the second cycle. The greater the irreversible portion of $\Delta R/R_o$, the greater was the fractional decrease in modulus. The strain sensitivity, given by the reversible portion of $\Delta R/R_o$ divided by the reversible strain, was 1.9 - 2.3 at all stress amplitudes for both Cycles 1 and 2. The $\Delta R/R_o$

Table 1 Electromechanical behavior under static tension. (Data correspond to Fig. 2a.)

Strain (%)	$\Delta R/R_o$ (10^{-3})		Strain sensitivity[+]	
	Measured	Calculated*	Measured	Calculated
0.40	7.4	6.2	1.9	1.5
0.50	8.8	7.7	1.8	1.5
0.60	11	9.2	1.8	1.6
0.70	13	10	1.9	1.6
0.80	14	12	1.8	1.6
0.90	16	14	1.8	1.6
1.0	19	16	1.9	1.6
1.1	21	17	1.9	1.6

* Calculated from change in dimensions.

$$\frac{\Delta R}{R} = \frac{1+\varepsilon}{1-2\nu\varepsilon} - 1, \text{ where } \varepsilon \text{ = strain and } \nu = \text{Poisson's ratio} = 0.27$$

[+] $\Delta R/R_o$ divided by the strain.

calculated from the change in dimensions was less than the measured reversible $\Delta R/R_o$ at every stress amplitude.

Comparison of the calculated and measured reversible $\Delta R/R_o$ shows that dimensional change is the main cause of the observed reversible resistance change. However, dimensional change does not account for all of the observed reversible resistance change. A reversible structural change that gives rise to a resistivity change may contribute to the cause. A structural change upon tension of heat-treated benzene-derived graphite fibers had been suggested by Raman scattering [4].

The observed irreversible resistance change is

Table 2 Electromechanical behavior under cyclic tension

Maximum stress / fracture stress	18.8%[a]	38.5%[a]	58.1%[b]	73.1%[b]	83.0%[c]
Strain (%)					
Reversible					
Cycle 1	0.22±0.02	0.41±0.05	0.65±0.08	0.73±0.10	0.86±0.10
Cycle 2	0.22±0.02	0.41±0.06	0.65±0.10	0.72±0.13	0.85±0.12
Irreversible					
Cycle 1	0.00+0.00	0.00+0.00	0.00+0.00	0.04±0.01	0.05±0.02
Cycle 2	0.00+0.00	0.00+0.00	0.00+0.01	0.05±0.01	0.07±0.02
DR/R_o (10^{-3})					
Reversible					
Cycle 1	5.00±0.55	7.80±0.73	12.51±1.11	14.61±1.61	18.40±2.51
Cycle 2	5.00±0.64	7.80±0.92	12.50±1.23	14.58±1.82	18.13±2.84
Irreversible					
Cycle 1	0.00±0.00	0.00±0.00	1.50±0.21	2.20±0.33	4.00±0.78
Cycle 2	0.00±0.00	0.00±0.01	1.52±0.32	2.27±0.54	4.65±0.93
Calculated [+]	3.4	6.3	10.0	11.9	14.1
Strain sensitivity*					
Cycle 1	2.27±0.13	1.90±0.76	1.92±0.13	2.00±0.21	2.14±0.19
Cycle 2	2.27±0.14	1.90±0.85	1.92±0.12	2.03±0.22	2.13±0.20
Elastic modulus (GPa)					
1st cycle	230	226	228	221	225
2nd cycle	229	225	225	214	213
Fractional decrease in modulus from 1st cycle to 2nd cycle	0	0	1%	3%	5%

[+] Calculated from change in dimensions.

$$\frac{\Delta R}{R} = \frac{1+\varepsilon}{1-2\nu\varepsilon} - 1, \text{ where } \varepsilon \text{ = strain and } \nu = \text{Poisson's ratio} = 0.27$$

* Reversible $\Delta R/R_o$ divided by the reversible strain.

[a] 5 samples tested. [b] 4 samples tested. [c] 3 samples tested.

attributed to damage, as supported by the accompanying decrease in the elastic modulus. Damage occurs at stress amplitudes ≥ 58.1% of the fracture stress and increases with increasing stress amplitude. Irreversible strain occurs at stress amplitudes ≥ 73.1% of the fracture stress and increases with increasing stress amplitude. Thus, damage occurs not only when there is irreversible strain, but also at a stress amplitude of 58.1% of the fracture stress, at which the strain is totally reversible. This suggests that damage can occur even in the regime of elastic deformation.

The strain sensitivity values given in Table 1 are slightly lower than those of Table 2 because the total strain was considered in Table 1 and the reversible strain was considered in Table 2. Nevertheless, in both cases, the strain sensitivity is quite independent of strain/stress for essentially the whole range of strain/stress up to fracture. The strain sensitivity values are higher than the values in the range 1.3 - 1.7 reported in [1] (probably due to the difference in carbon fiber), but are close to those in the range 1.95 - 2.02 reported in [2].

Even at a stress amplitude of 83.0% of the fracture stress, the irreversible portion of $\Delta R/R_o$ is much smaller than the reversible portion. Therefore, the use of the carbon fiber as a strain/stress sensor is possible. The irreversible portion, on the other hand, can be useful as an indicator of the amount of damage, so that the carbon fiber becomes a sensor of its own damage. This damage should be distinguished from fiber breakage, which would cause the irreversible $\Delta R/R_o$ to be ∞. The increase in the irreversible portion of $\Delta R/R_o$ with cycle number suggests the possibility of the fiber to monitor its own fatigue damage, though fatigue testing was not conducted in this work.

Strain sensitivities similar to those in Table 1 were obtained upon static tension using Amoco's Thornel P-25-X carbon fibers (11 μm diameter, 0.9% ultimate elongation, 160 ± 8 GPa tensile modulus, 1.4 ± 0.4 GPa tensile strength and (6.1 ± 0.7) x 10^{-4} Ω.cm resistivity) instead of Torayca T-300. For P-25-X, the measured strain sensitivity at 0.2 - 0.7% strain ranged from 1.8 to 1.9 and the calculated values ranged from 1.5 to 1.6.

In summary, this work showed that (i) the electromechanical behavior of carbon fiber is not totally reversible when the tensile stress is ≥ 58.1% of the fracture stress, though the irreversible resistance change is small compared to the reversible resistance change, (ii) the reversible resistance change is mainly due to the dimensional change associated with elastic deformation, though the dimensional change cannot explain the entire reversible resistance change, (iii) the irreversible resistance change is associated with an irreversible decrease in the tensile modulus and, in most cases, is also associated with an irreversible strain, (iv) the irreversible resistance change increases with tensile stress and increases slightly with tensile cycle number (from 1 to 2), (v) the irreversible resistance increase is attributed to fiber damage, and (vi) the strain sensitivity (reversible $\Delta R/R_o$ per unit reversible strain) is 1.9 - 2.3 and is quite independent of stress or cycle number (from 1 to 2).

Acknowledgement - This work was supported in part by Center for Electronic and Electro-Optic Materials of the State University of New York at Buffalo.

REFERENCES

1. Conor, P.C. and Owston, C.N., *Nature*, 1969, **223**, 1146.
2. Owston, C.N., *J. Physics, D*, 1970, **3**, 1615.
3. Berg, C.A., Cumpston, H. and Rinsky, A., *Textile Research Journal*, 1972, **42**(8), 486.
4. DeTeresa, S.J., *Carbon*, 1991, **29**, 397.
5. Crasto, A.S. and Kim, R.Y., *Proc. Am. Soc. Composites, 8th Tech. Conf.*, Technomic Pub. Co., Lancaster, PA, 1994, pp. 162-173.
6. Wang, X. and Chung, D.D.L., *Smart. Mater. Struct.*, in press.
7. Sakata, H., Dresselhaus, G., Dresselhaus, M.S. and Endo, M., *J. Appl. Phys.*, 1988, **63**, 2769.

Optomechanical actuation using intercalated graphite

M.S. Salib, A. Petrou and D.D.L. Chung
Center for Electronic and Electro-Optic Materials
State University of New York at Buffalo, Buffalo NY 14260-4400 USA

(Received 13 February 1997; accepted in revised form 3 March 1997)

Key Words - A. Intercalation compounds, D. optical properties, mechanical properties

Smart materials comprise materials that have one or both of the following functions - sensing and actuation. Sensing refers to the sensing of strain or stress, while actuation refers to providing strain or stress. The signal sensed and the signal that actuates can be electrical, magnetic or optical. For example, piezoelectric, piezoresistive, electrostrictive and electrorheological effects involve an electrical signal; magnetostrictive and magnetorheological effects involve a magnetic signal; while optical fibers and the photoelastic effect involve an optical signal.

A relatively new effect is the electromechanical effect in intercalated graphite. This effect involves the reversible expansion of intercalated graphite by up to 4500% parallel to the c-axis upon passing an electric current in the same direction; the equivalent stress generated is up to 3 MPa [1,2]. In other words, intercalated graphite is an actuator that responds to an electrical signal, which heats the sample, thereby causing reversible exfoliation expansion, at 100°C in the case of graphite intercalated with bromine [3]. The heating may be provided by an optical beam instead. The use of

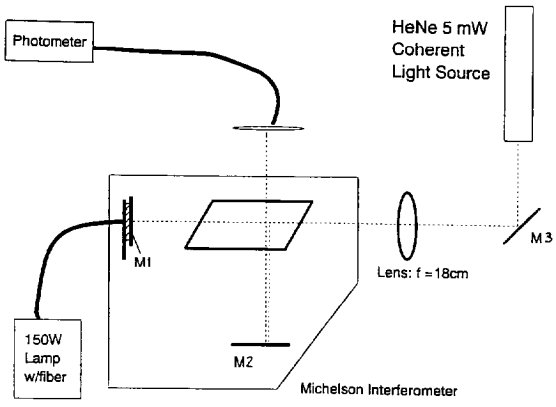

Fig. 1. Set-up for optomechanical testing.

infrared and laser heating methods had been previously used for irreversible exfoliation [4], but not for reversible exfoliation. Reversibility is essential for switching. The optomechanical effect is expected to be practically useful for adaptive optics, optically controlled movement and smart thermal/electrical contacts. In this work, the optomechanical switching was observed and characterised.

The sample used was a graphite-bromine residue compound based on highly-oriented pyrolytic graphite (HOPG), of size 4.2 x 3.3 x 1.0 mm, and containing 1.9 mol% Br_2. Intercalation was carried out by exposure to bromine vapor in air at room temperature to attain stage 2, followed by intercalate desorption below 100°C. The optomechanical effect was observed by directing unfocused 400-500 mW white light (150 W tungsten-halogen lamp, via an optical fiber bundle of diameter 3 mm) onto the sample (4.2 x 3.3 mm) and measuring the strain optically during irradiation switching. The set-up (Fig. 1) consisted of a Michelson interferometer in which the moveable lightweight mirror M1 was mounted on the sample being studied. The second mirror (M2) was stationary. The sample surface perpendicular to the c-axis was illuminated from the back by the white light, which induced a change δz in the near-surface sample thickness along the c-axis. Mirror M1 traveled by the same amount toward the beam splitter and caused the movement of $2\delta z/\lambda$ interference fringes on the photo-diode detector, which were recorded by the counter. A weak (5 mW) He-Ne laser (λ = 6328 A)

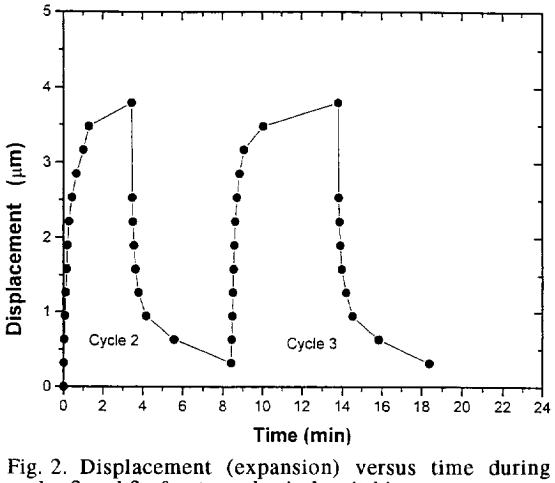

Fig. 2. Displacement (expansion) versus time during cycles 2 and 3 of optomechanical switching.

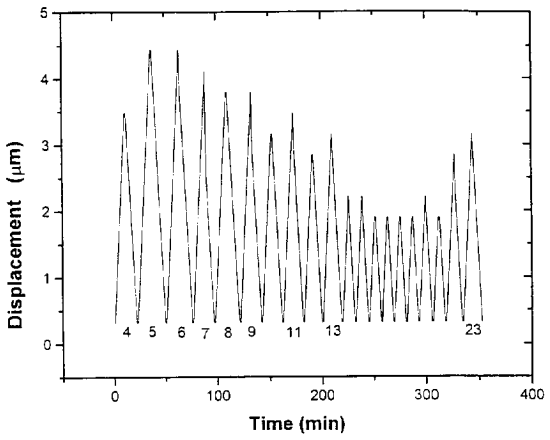

Fig. 3. Displacement (expansion) versus time during cycles 4 - 23 of optomechanical switching.

was used as a probe beam for the observation of the interference fringes so as to measure the amount of expansion or contraction. The resolution in δz was 500Å.

The whole sample expanded uniformly and reversibly along the c-axis during light irradiation, as shown in Fig. 2 for cycles 2 and 3 and in Fig. 3 for cycles 4 - 23. Upon removal of the light irradiation, the contraction along the c-axis was also uniform. Even though the light beam size was smaller than the sample size, the whole sample expanded. This is due to the high in-plane thermal conductivity. Only the limited depth of the sample near the irradiated surface expanded as the expansion was less than 5 μm. The expansion varied from cycle to cycle, as shown in Fig. 3, probably because of the slight variation of the depth of optical heating from cycle to cycle. The rise/fall time was 15 s for the main (initial) parts of the rise and fall. No correlation was found between the expansion and the intercalate concentration.

Irradiation using an argon-ion laser beam (wavelength = 5145 Å at a power of 400 mW) instead of white light gave results similar to Figs. 2 - 3. Upon increasing the argon laser power (from 0 to 1 W), no change of the fringe shape was observed. This means that the sample underwent negligible dimensional change in the in-plane directions during the expansion along the c-axis.

The observed optomechanical effect differs from the related electromechanical effect in the same material [1,2] in that the expansion is much larger, and the fall and rise times are much shorter in the latter. The large expansion in the electromechanical effect is because the whole thickness of the sample expanded. The short rise time in the electromechanical effect is because direct Joule heating rather than optical heating was involved. In spite of the low expansion and long rise and fall times in optomechanical switching, the phenomenon is attractive in its requiring no electrical contacts, in contrast to this requirement in electromechanical switching. This makes it easier to implement.

In conclusion, optomechanical actuation was achieved reversibly using highly oriented pyrolytic graphite intercalated with bromine (1.9 mol% Br_2). White light from a 150 W tungsten-halogen lamp was used for optomechanical switching. The displacement was ~4 μm and occurred only along the c-axis of the graphite and for the limited depth of the sample near the

irradiated surface. The expansion was uniform across the whole plane perpendicular to the c-axis, even though the switching beam was smaller than this plane. The rise and fall times were ~15 s. The origin of the optomechanical effect is the reversible exfoliation of the near surface region of the intercalated graphite.

REFERENCES

1. Chung, D.D.L. and Wong,, L. W., *Carbon*, 1986, **24**, 639.
2. Chung, D.D.L., *Smart Mater. Struct.*, 1992, **1**, 233.
3. Chung, D.D.L., *J. Mater. Sci.*, 1987, **22**, 4190.
4. Hirschvogel, A. and Zimmermann, H., European Patent Application, EP 87 489, 1983.

Discussion of the formation of nanometric texture in spherical carbon bodies

M. INAGAKI
Faculty of Engineering, Hokkaido University,
Kita-ku, Sapporo 060, Japan

(Received 15 January 1997; accepted in revised form 28 February 1997)

Key Words - A. carbon black, mesophase, B. pyrolysis, D. texture

One of characteristics of carbon materials is a wide variety of texture. The author has presented a proposal to classify the texture on a nanometric scale on the basis of the scheme and the degree of preferred orientation of the hexagonal carbon layers of basic structural units (BSUs), as shown in Fig. 1 [1,2]. These textures are known to govern the graphitization behavior [3] and also various properties [2]. In axial and point orientation schemes, carbon layers are preferentially oriented along the reference axis and point, respectively, and result in the formation of various carbon fibers and carbon spheres. In these orientation schemes, radial and concentric arrangements of the carbon layers are possible (Fig. 1). In practice, it is well known that the mesophase-pitch-based carbon fibers can have different textures such as radial and concentric textures in their cross-sections. In carbon blacks, carbon layers are oriented statistically in a concentric manner, as can be seen in various structural models in which the details of the arrangement of each layer are little different from each other. In mesophase spheres, however, the orientation scheme of carbon layers is known to be radial, at least near the surface, as many authors have confirmed since Brooks and Taylor [4].

However, there has been no explanation and even no discussion on the reason why these textures are formed, as far as the author is aware. Why do most of the mesophase spheres have a Brooks-Taylor type texture and why not a concentric one? Why do the carbon blacks have a concentric texture, in contrast to the mesophase spheres?

In this note we shall discuss the reason why these two kinds of arrangement of carbon layers, radial and concentric, are possible by focusing on spherical carbon bodies.

In Table 1, a brief description of the formation conditions and the phases involved at the interface between carbon spheres and their surroundings during thermal decomposition and subsequent carbonization processes are summarized, together with the resultant texture in carbon spheres in six different materials.

The spherical carbon bodies can be classified into three from their nanometric texture, concentric, radial and random arrangements of carbon layers. If we draw our attention to the interface between the sphere and its surroundings at the moment of formation, we can understand that the concentric texture in spherical bodies is caused always when the interface between different phases is either liquid/gas, solid/liquid or solid/gas. On the other hand, the formation of carbon spheres with radial texture occurs with a liquid/liquid interface. This correspondence seems to be reasonable because of a strong interaction between the spheres and their surroundings during their formation.

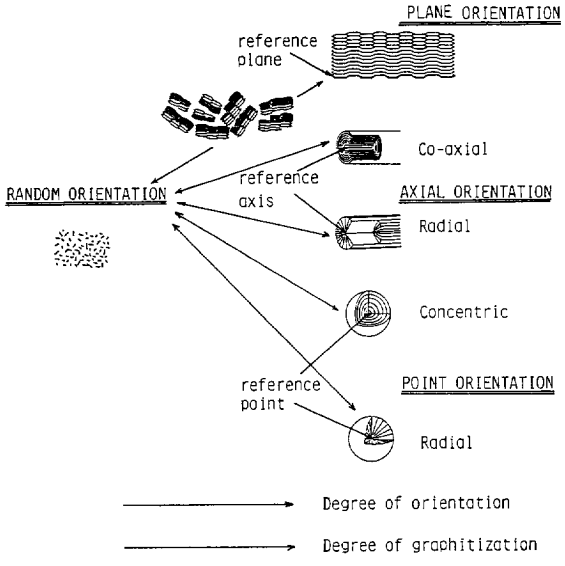

Fig. 1 Classification of nanometric texture in carbon materials based on the preferred orientation of the carbon layers in BSUs.

The fundamental theory of nucleation and growth of crystals tells us that the critical radius of a nucleus depends on the interfacial energy. This interfacial energy is related strongly to the difference in surface energies between the two phases in contact at the interface. During the formation of these spherical particles, BSUs are composed of a parallel stacking of condensed aromatic rings. In these units, the anisotropy may be supposed to be similar to that in graphite layers. If so, the basal plane of BSUs has much lower surface energy than the edge plane.